by K. Sandeep[1]†, R. Shankar[1], A.K. Warrier[1‡], and W. Balsam[2]*

Diffuse reflectance spectroscopy of a tropical southern Indian lake sediment core: A window to environmental change

[1] Department of Marine Geology, Mangalore University, Mangalagangotri-574 199, India; *Corresponding author,
E-mail: sandeepk01@gmail.com
[2] Department of Earth Sciences, Dartmouth College, Hanover, NH 03755, USA

(Received: December 17, 2015; Revised accepted: July 9, 2016)

http://dx.doi.org/10.18814/epiiugs/2017/v40i1/017007

Pookot is a small freshwater lake situated in the Sahyadri (the Western Ghat) of southern India. We used diffuse reflectance spectroscopy (DRS) and magnetic parameters to characterize the sediment components present in a core dating back to ~3000 cal. years B.P. DRS data indicate the presence of $CaCO_3$, goethite, hematite/goethite, clay minerals and organic carbon in the lake sediments. Based on the down-core variations of the four components, and the values of χ_{lf} (low-field magnetic susceptibility indicative of detrital magnetite) and DRS parameter redness %, we reconstructed the paleoenvironmental history of the region surrounding the lake. The down-core variations of DRS-determined sediment composition and of data obtained from independent analyses ($CaCO_3$, S-ratio, clay % and C_{org} %) are similar. The pre-2500 cal. years B.P. period was characterized by a stronger monsoon compared to the Present. From 2500–1000 cal. years B.P., the monsoon was weak and steady, but interspersed with brief periods of strong monsoon, whereas from 1000 cal. years B.P. to the Present, rainfall exhibited a fluctuating trend. Rainfall was relatively high during the Medieval Warm Period (1000–600 cal. years B.P.), low during the Little Ice Age (600–350 cal. years B.P.) and from 350 cal. years B.P. to the Present, it exhibited an increasing trend.

Introduction

A number of proxies and techniques have been applied to extract palaeoenvironmental information from lacustrine sediments, e.g., particle size (Conroy et al., 2008; Warrier et al., 2014a), rock magnetics (Shankar et al., 2006; Frank, 2007; Warrier et al., 2014b), geochemistry (Oliveira et al., 2009; Warrier and Shankar, 2009), organic matter (Meyers and Lallier-Verges, 1999; Chengjun et al., 2010), pollen (Trivedi and Chauhan, 2008; Lee et al., 2010), oxygen and carbon isotopes (Beuning et al., 2003; Leng and Marshall, 2004) etc. However, diffuse reflectance spectroscopy (DRS) has emerged during the recent years as a new tool for quantifying the sediment colour rapidly and effectively. Visible reflectance spectra have been used to identify iron oxides and oxyhydroxides (Deaton and Balsam, 1991; Jiang et al., 2014), clay minerals and sediment organic content (Balsam and Deaton, 1991; Balsam et al., 1998). The technique has been successfully used on marine (Cortina and Herguera, 2014; Dong et al., 2014) and lake (Ji et al., 2005; Duan et al., 2014; Wei et al., 2014; Fang et al., 2015; Zhang et al., 2015) sediments to estimate the past climate; on soil, loess and paleosol deposits to understand pedogenesis (Lyons et al., 2014; Colombo et al., 2015; Srivastava et al., 2015; Mohanty et al., 2016), and for characterisation of aerosol particles (Arimoto et al., 2002). In this study, the first on lacustrine sediments in India using DRS, we investigate the use of spectrophotometric data to identify and evaluate components of the Pookot Lake sediments and to decipher past environmental changes.

Diffuse reflectance spectroscopy deals with the analysis of reflectance as a function of the wavelength of light diffusely reflected from a sample's surface (Balsam and Deaton, 1991). The advantages of this technique are that it is rapid, sensitive to some minerals, non-destructive and semi-quantitative. Visible (VIS) spectral reflectance techniques are especially sensitive to iron oxides and may be used to detect iron-bearing minerals at concentrations as low as 0.01% (Deaton and Balsam, 1991). The DRS technique is advantageous when compared to standard methods like XRD and Mossbauer spectroscopy. This is because the limits of resolution of XRD are higher than the amount of iron minerals commonly found in soil and sediment (Balsam et al., 2014), and Mossbauer spectroscopy just gives the ratio of iron species, not the actual amount. Iron oxide minerals like hematite and goethite are strong colouring agents and impart a yellowish/red colour to sediments. However, DRS technique is also sensitive to other components like carbonates, clay minerals and organic matter present in sediments. Therefore, visible reflectance spectra may be used to identify iron oxide and oxyhydroxide minerals (hematite and goethite), clay minerals (illite, mont-

Present address
†Department of Geology, Central University of Kerala, Tejaswini Hills, Periye (P.O.), Kasaragod, Kerala-671316, India
‡Department of Civil Engineering, Manipal Institute of Technology, Manipal University, Manipal-576104, India

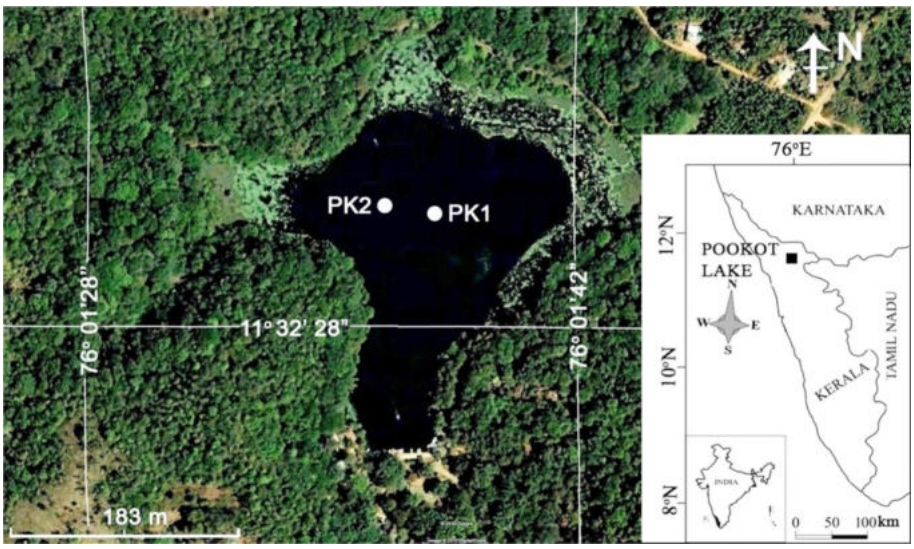

Figure 1. Satellite image of the Pookot Lake and surrounding areas (Source: Google Earth). Locations of sediment cores are shown as PK1 and PK2. Inset map shows the location of the lake in SW India.

morillonite and chlorite), calcite, and organic content (Balsam and Deaton, 1991; Deaton and Balsam, 1991; Balsam et al., 1998).

The main objective of this investigation is to reconstruct paleoenvironmental changes of the Pookot Lake area during the Late Holocene using the DRS technique. Only a few studies have been carried out on lake sediments from southern India and there is a dearth of high-resolution palaeoclimatic data for the region. To date, only one southern Indian lake has been studied for palaeoclimatic information (Shankar et al., 2006; Warrier and Shankar, 2009; Warrier et al., 2014a). However, there are thousands of lakes in southern India which may contain valuable palaeoclimatic information about the region. The present study aims to fill this lacuna and test the suitability of the DRS technique as a proxy for palaeomonsoons by comparing the results of DRS analysis with other data such as particle size, organic carbon and environmental magnetic data.

Study area

Pookot Lake (PK) is a closed, natural lake situated at an altitude of 775 m in the Sahyadri (the Western Ghat) near Vythiri in Wayanad District, Kerala (1132′30″N; 761′38″E; Fig. 1). The lake has a small catchment area (~0.74 sq.km) and a maximum water depth of 6.5 m. The main rock types in the PK catchment are hornblende-biotite gneiss and charnockite of Late Archaeozoic age (Geological and Mineral Map of Kerala, 1995; Soman, 1997). The primary soil type is ferruginous forest loamy soil with a dark reddish brown to black colour (Kerala Forest Department, 1986). The vegetation in the area is in the category of western tropical wet evergreen forests of low elevation (Bonnefille et al., 1999). The region experiences a tropical wet climate with an average rainfall of 4200 mm per year (India Meteorological Department, 2008). The relative humidity is on the average between 65 and 80% and the mean annual temperature range is 21–38 °C (Kerala Forest Department, 1986; Chandran, 2003).

Materials and methods

Two undisturbed sediment cores (PK1 and PK2) were collected from the Pookot Lake in November 2007 by manually pushing PVC pipes (diameter: 1.5 inches) into the sediment. To accommodate a water depth of 6.5 m, two PVC pipes (of 5 m length each and 3.8 cm diameter) were joined together for the coring exercise. The resulting cores obtained are 2.4 m and 2.2 m long (PK1 and PK2). This paper is based on the results obtained for core PK1 which was sampled at 0.5 cm interval (approximately 2 to 2.5 gram each).

Carbon-14 dating by accelerator mass spectrometry (AMS) was carried out on the organic matter of bulk sediment samples from selected depths at the Xi'an Accelerator Mass Spectrometer Center, Institute of Earth Environment, Chinese Academy of Sciences (CAS), China. The chronology of the two sediment cores (PK1 and PK2) was provided by 10 accelerator mass spectrometric (AMS) ^{14}C dates. Four ^{14}C dates are available for core PK1 and six for core PK2. The ^{14}C ages were calibrated using the code clam (Blaauw, 2010), which runs on open source software 'R' (R Development Core Team, 2010) and uses IntCal09.^{14}C calibration curve (Reimer et al., 2009). The age was calculated for every depth (0.5 cm) using a linear interpolation model with calibrated ages. Further details of chronology and age-depth model are provided in Sandeep et al. (2015).

Sediment samples were prepared following standard techniques for magnetic susceptibility measurement (Walden, 1999). Samples were dried in a hot air oven at 35 °C and gently disaggregated using an agate mortar and a pestle. They were placed in plastic bags and tightly packed in 8-cc non-magnetic plastic bottles. Magnetic susceptibility at low frequency (0.47 kHz; χ_{lf}) was determined using a Bartington Susceptibility Meter with a dual-frequency sensor (Model MS2B). Isothermal remanent magnetisation (IRM) was induced in the samples at different field strengths (20, 60, 100, 300, 500 and 1000 mT) using a Molspin pulse magnetiser. The isothermal remanence induced at 1T field (the maximum field attainable in the Environmental Magnetism Laboratory at Mangalore University) was considered as saturation isothermal remanent magnetisation (SIRM). The remanence acquired was measured using a Molspin spinner fluxgate magnetometer. Using the remanence measurements, values of S-ratio and HIRM were calculated. S-ratio is the ratio between IRM_{300mT} and SIRM whereas HIRM is the difference between SIRM and IRM_{300mT}. The S-ratio used in this study is the forward field S-ratio (Kruvier and Passier, 2001; Heslop, 2009) and not the classical back field S-ratio proposed by Stober and Thompson (1979).

Diffuse reflectance spectroscopic analysis was carried out on 30 representative samples. Sample preparation followed the procedures described by Balsam and Deaton (1991). The sediment sample was ground and made into slurry on a glass micro slide with distilled water. Then it was smoothed and dried slowly at low temperature (< 40 °C) and analysed on a Perkin-Elmer Lambda 6 spectrophotometer with a

diffuse reflectance attachment (reflectance sphere) from near ultra violet (NUV-250-400 nm) through visible (VIS-400-700 nm) to the near infrared (NIR-700-850 nm) region. The sediment slides were photographed for visual comparison. The samples were scanned at a rate of 600 nm/min and % reflectance values were recorded relative to a white barium sulphate standard at 1 nm intervals. Reflectance data were processed to obtain percent reflectance in standard colour bands, i.e., violet = 400~450 nm, blue = 450~490 nm, green = 490~560 nm, yellow = 560~590 nm, orange = 590~630 nm, red = 630~700 nm. Percent reflectance in these colour bands was calculated by dividing the percentage of reflectance in a colour band by the total reflectance of the sample in the VIS. Total reflectance, except for scaling, is the same as L* or optical lightness (Balsam et al., 1999). In this paper total reflectance of a sample will be refered to as optical lightness. Data from the spectrophotometer were recorded at 1 nm interval from 250 to 850 nm. To enhance the variability of percent reflectance spectra, the first derivative (% reflectance per nanometer) at a 10-nm wavelength interval was calculated. The first derivative curves, calculated as percent per nanometer and plotted at the mid-points of the 10 nm calculation intervals, are more amenable to interpretation than the untransformed reflectance spectra. Simultaneous R- and Q-mode factor analysis was carried out on first-derivative values for all the samples using SPSS v. 16 for Windows. Factor analysis was carried out to extract assemblages that can be interpreted in terms of mineral composition. Factors were extracted using principal component analysis and redistributed using varimax rotation which was employed to maximise the variance between the variables.

Organic carbon content was determined for 26 samples. Bulk sediment samples were dried in a hot air oven at 40 °C and finely ground and homogenized using an agate mortar and pestle. About 2 g of the powdered sample was treated with 1N HCl that was added in small increments until effervescence stopped (Schumacher, 2002). It was later allowed to react at room temperature overnight to facilitate complete dissolution of carbonates. The sample was then washed 3–4 times with deionised water and dried in a hot air oven at 100 °C. Weight loss after the HCl treatment gave the weight of $CaCO_3$ or inorganic carbon and is expressed as percentage. After the removal of inorganic carbon, the remaining carbon is organic. The organic carbon in the decarbonated samples was determined using a CHNS analyzer (Model: Elementar Vario EL III; Liying et al., 2009).

Results and discussion

Colour and magnetic susceptibility data

Figure 2 depicts the colour and magnetic susceptibility data (as bars) of Pookot Lake sediments. A visual observation of the sediment colour reveals that samples with higher χ_{lf} values generally correlate with darker sediment. Colour variation in sediments is determined by the relative concentrations of a variety of sediment components including organic matter, carbonate, clay and iron oxides (Ji et al., 2005). However, the identification of low concentrations of hematite is difficult through visual examination because it is sensitive to masking by other sediment components, especially organic matter (Balsam and Damuth, 2000). In general, high χ_{lf} values indicate periods of high rainfall (Shankar et al., 2006; Balsam et al., 2011 and references therein; Sandeep et al., 2015). High rainfall leads to a high detrital influx which, in the study area, leads to a high concentration of detrital magnetite in the samples. Detrital influx may also be related to changes in catchment erosion which, in turn, is related to rainfall.

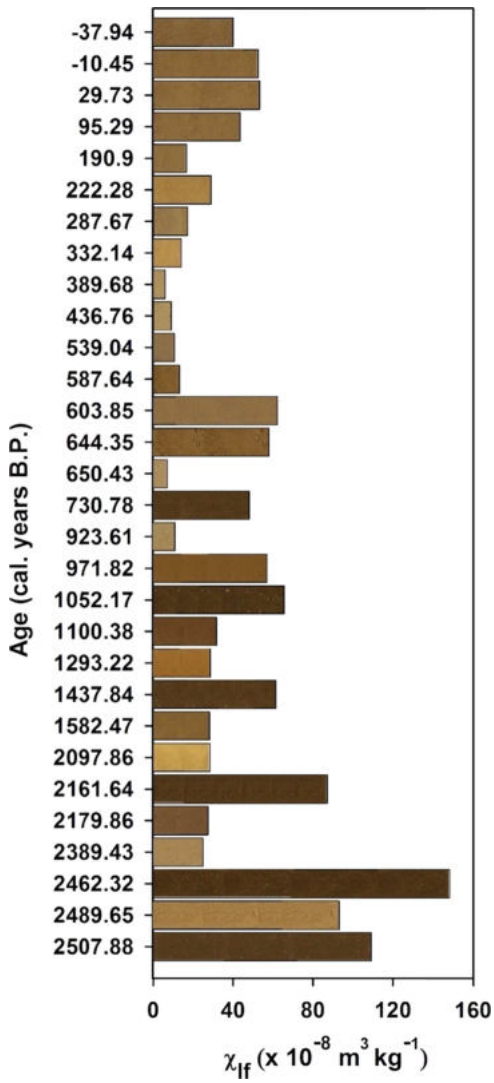

Figure 2. Sediment colour of selected samples of Pookot Lake sediments. Length of the bar indicates the value of magnetic susceptibility. Note: In general, samples with high susceptibility are dark.

Percentage reflectance, percentage redness and first derivative values

Percentage reflectance of sediments is closely associated with the presence of light and dark sediment components in samples. The presence of light components like carbonate and kaolinitic clay increases the brightness of the sample, thereby enhancing the reflectance. On the other hand, the presence of dark components like hematite/goethite or organic matter decreases the brightness and, therefore, the reflectance (Ji et al., 2001). When more than one component is present in a sample, the net effect of the components determines the reflectance.

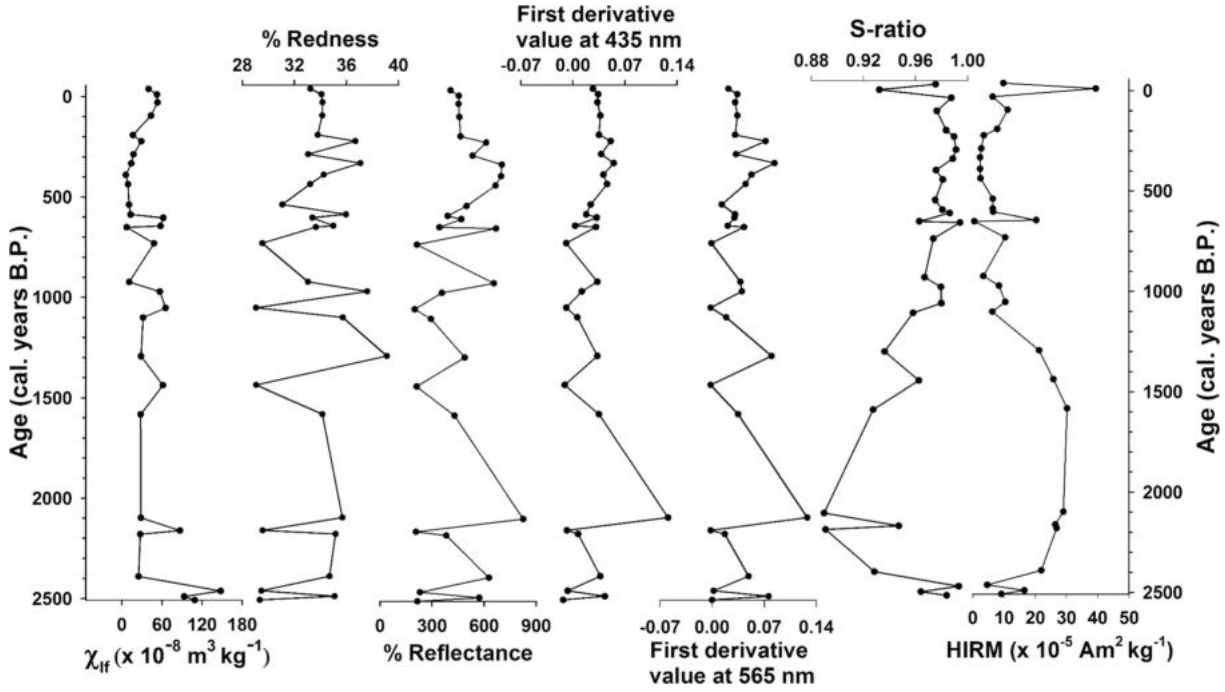

Figure 3. Magnetic susceptibility (χ_{lf}), % redness, optical lightness, first derivative values at 435 nm and 565 nm, S-ratio and HIRM values for selected samples from the Pookot Lake sediment core PK1.

Table 1. Correlation matrix for χ_{lf}, S-ratio, HIRM, percentage reflectance values (in violet, blue, green, yellow, orange, red), total percentage reflectance (optical lightness) and 1st derivative values at 435 nm (Gt435) and 565 nm (Hm565)

	χ_{lf}	S-ratio	HIRM	% Violet	% Blue	% Green	% Yellow	% Orange	% Red	Optical lightness	Gt435	Hm565
χ_{lf}	1.00											
S-ratio	0.11	1.00										
HIRM	0.17	**–0.83**	1.00									
% Violet	**0.54**	0.22	–0.02	1.00								
% Blue	**0.47**	0.26	–0.05	**0.99**	1.00							
% Green	0.18	0.25	–0.09	**0.66**	**0.74**	1.00						
% Yellow	–0.37*	–0.21	0.10	**–0.83**	**–0.80**	–0.23	1.00					
% Orange	–0.43**	–0.24	0.08	**–0.97**	**–0.98**	**–0.64**	**0.89**	1.00				
% Red	**–0.48**	–0.24	0.02	**–0.94**	**–0.96**	**–0.86**	**0.61**	**0.90**	1.00			
Optical lightness	**–0.63**	–0.12	–0.17	**–0.73**	**–0.68**	–0.16	**0.77**	**0.71**	**0.56**	1.00		
Gt435	**–0.48**	–0.29	0.05	**–0.77**	**–0.74**	–0.18	**0.94**	**0.81**	**0.56**	**0.88**	1.00	
Hm565	–0.39*	–0.29	0.05	**–0.85**	**–0.86**	**–0.50**	**0.87**	**0.91**	**0.74**	**0.84**	**0.90**	1.00

Numbers marked in bold are significant at 1% level, * = 5%, ** = 2%.

Down-core variations of percent reflectance, percent redness, and values of first derivative at 435 nm indicative of goethite (Gt435) and 565 nm indicative of hematite (Hm565) (Deaton and Balsam, 1991), S-ratio and HIRM are shown in Figure 3. The correlation matrix for these parameters is given in Table 1. Percentage reflectance exhibits significant down-core variations from 20 to 82.5%. It shows a negative correlation with χ_{lf} ($r = –0.63$; $p < 0.01$; $n = 30$), suggesting that periods of high values of χ_{lf} were characterised by low values of reflectance and vice versa. This relationship is also apparent from a visual examination of sediment colour (Fig. 2).

We calculated the first derivative of percentage reflectance because most untransformed percentage reflectance curves are almost featureless and exhibit few peaks. The first derivative curves exhibit peaks wherever the rate of change of raw spectral value is high but are flat when the rate of change is minimal (Balsam and Deaton, 1991). Figure 4 depicts the first derivative values versus wavelength for Pookot Lake samples. Peaks are indicative of a variety of components, especially hematite, goethite, clay minerals, carbonate and organic matter. Hematite and goethite have distinct peaks in the VIS reflectance spectra (Deaton and Balsam, 1991). The characteristic peak for hematite is centred at 565 nm, but may range from 555 nm at low concentrations (weight percent 0.05%) to 575 nm at high concentrations (> 1%).

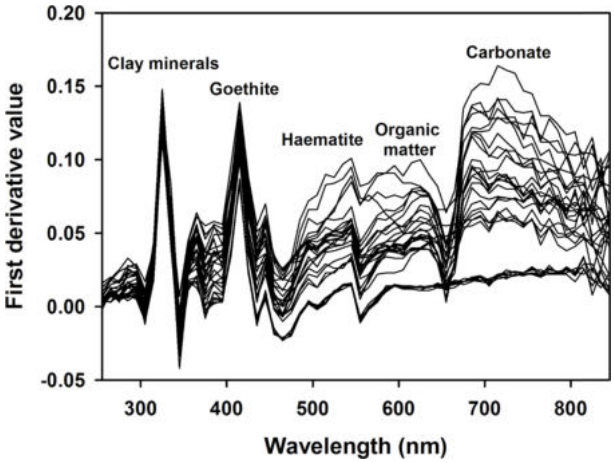

Figure 4. First derivative value vs. wavelength for Pookot Lake sediment samples. Note: The peaks are indicative of different mineral components in the samples.

Goethite has two peaks, one at 535 nm and the other at 435 nm. In practice, the 435 nm peak is a better indicator of goethite because the 535 nm peak is frequently obscured by hematite (Balsam and Wolhart, 1993; Balsam and Damuth, 2000). However, the goethite peak may also vary slightly, depending on changes in concentration, substituted metal ions (Torrent and Barron, 2002), and/or matrix (Balsam and Deaton, 1991). All the PK samples exhibit a major peak at 415 nm and a smaller one at 445 nm indicative of goethite. The peak at 545 nm indicates the presence of hematite in low concentrations. In addition, three more peaks at 325 nm, 595–625 nm and 685–745 nm were documented. The one in the near ultra-violet at 325 nm is identified as clay minerals (montmorillonite and illite). The broad peak around 595–625 nm (the red end of the spectrum) is probably indicative of organic matter and the broad peak at 685–745 nm suggests carbonate (Balsam and Deaton, 1991; Balsam and Beeson, 2003).

Magnetic susceptibility exhibits a significant positive correlation with % violet and % blue but negative correlation with % yellow, % orange, % red, optical lightness, Gt435 and Hm565. Magnetic susceptibility exhibits negative correlation with % redness ($r = -0.48$, $p < 0.01$, $n = 30$) and Hm565 ($r = -0.39$, $p = 0.03$, $n = 30$). This may be because haematite exhibits relatively low values of magnetic susceptibility compared to magnetite. Hence, a relative increase in the proportion of haematite with respect to magnetite/maghemite decreases the χ_{lf} values. It is also possible that magnetite/maghemite may be oxidized to haematite. Percent redness varies from 29 to 39% whereas Hm565 values range from –0.002 to 0.128. Redness of a sediment sample is primarily related to the iron oxide concentration, especially hematite and goethite (Deaton and Balsam, 1991; Ji et al., 2001). The presence of hematite and goethite not only reduces reflectance, but also increases redness. Goethite is yellowish-brown and hematite dark red. Periods with high χ_{lf} values are characterised by low % redness values and vice versa. It is interesting to note that when the optical lightness values increase, percentage redness also increases. There is a positive correlation between optical lightness and % redness ($r = 0.54$, $p < 0.01$. $n = 30$). If solely hematite or goethite were present in the samples, the contrary would have been expected (i.e., a negative relationship) because as the abundance of dark minerals like hematite or goethite increases, reflectance decreases and vice versa. A positive relationship between them indicates that reflectance and sediment colour are not controlled exclusively by the hematite/goethite content but also by additional components.

The peaks in optical lightness and Hm565 correspond to troughs in S-ratio values and vice versa ($r = -0.29$, $p > 0.05$, $n = 30$). The Gt435 values, indicative of goethite, are also negatively correlated with χ_{lf} ($r = -0.48$, $p < 0.01$, $n = 30$), indicating the intimate association between hematite and goethite in the region. The close association of hematite with goethite in tropical conditions is well documented (Cornell and Schwertmann, 1996).

Factor analysis

Factor analysis is generally used to explore multivariate relationships in data sets and to group a large number of associated variables into a small number of factors. Factor analysis of the first derivative values of Pookot Lake sediment samples (using Principal Component Analysis) extracted four factors with eigenvalues greater than one. The four factors explain 93% of the cumulative variance. The individual variance explained by Factors 1 to 4 is 63.9%, 19.8%, 6.1% and 3.1% respectively. The factor pattern diagrams (Fig. 5) which plot the importance of each wavelength (factor loading) through the wavelength range analyzed was compared to the first-derivative curves for known minerals and combinations of minerals. The loadings for each factor describe how each of the sixty variables (first derivative wavelengths) contributed to that factor. The higher the value of loading, the more significant its contribution to a factor is (Balsam and Wolhart, 1993; Balsam and Deaton, 1991). Down-core variations of factor scores (Fig. 6) indicate temporal variations in the minerals represented by that factor.

Factor 1

Factor 1 is a positive factor and has the highest loadings from 675 to 845 nm with a maximum value of 0.97. Two small secondary peaks are centered at 455 and 635 nm. The pattern is similar to that of the carbonate factor identified by Balsam and Deaton (1991) and Balsam and Damuth (2000). Hence, this factor is interpreted as the carbonate factor (Fig. 5a). This interpretation is supported by carbonate data. Down-core variations of Factor 1 pattern and carbonate percentage (Fig. 6) are similar despite the fact that the samples used for carbonate analysis and DRS are not from the same depths. For this reason, the correlation coefficient between the two variables could not be obtained. There is also a positive correlation ($r = 0.44$; $p = 0.02$; $n = 30$) between factor 1 and percentage reflectance. The scores for Factor 1 range from –1.16 to 3.87. High positive values are documented for periods of low χ_{lf} value and high carbonate (= periods of low rainfall). On the other hand, low negative values are recorded for periods of high χ_{lf} value and low carbonate % (= periods of high rainfall). This factor has a negative correlation coefficient with χ_{lf} ($r = -0.67$, $p < 0.01$, $n = 30$). It may be noted that carbonate percentage also exhibits a correlation coefficient of –0.51 ($p < 0.01$, $n = 26$) with χ_{lf}.

Factor 2

Factor 2 is bimodal and also a positive factor. It has the highest

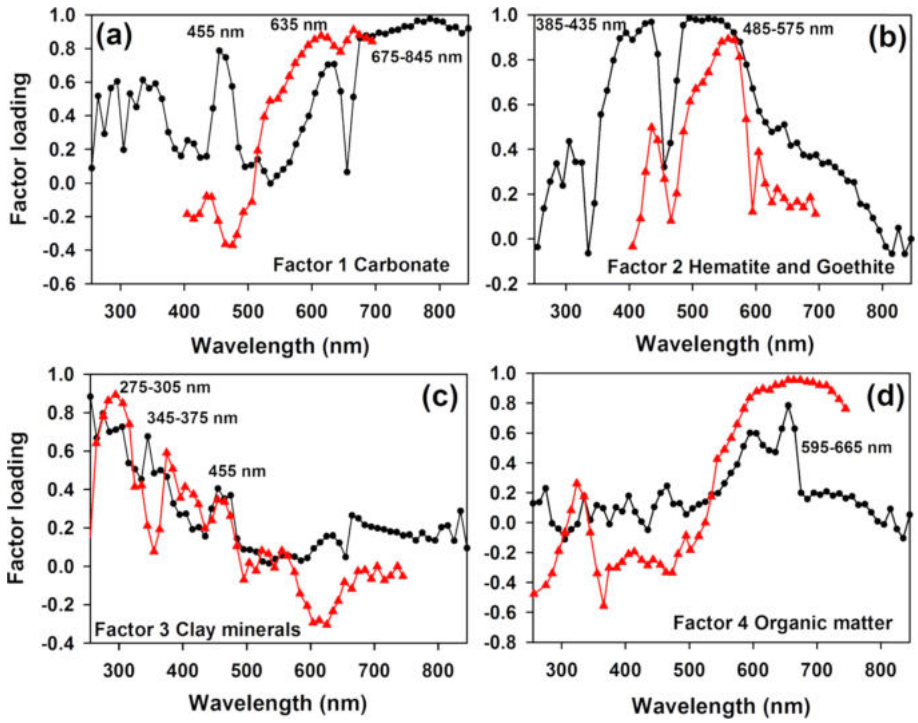

Figure 5. Factor-pattern curves. Note: The curves (describing how important each wavelength is in each factor) were derived from analyzing the full spectral data set. This data set encompasses 30 samples and, for each sample, there are 60 first derivative values calculated at the midpoint of the 10-nm sample interval from 250 to 850 nm. A varimax rotation was carried out before factor extraction and the factors are listed in the order of decreasing variance explained. Four factors were extracted with eigenvalues greater than one. They are identified as carbonates, hematite/goethite, clay minerals and organic matter. Those in red are factor-pattern curves for similar factors identified by Balsam and Damuth (2000) and Damuth and Balsam (2003).

loadings from 385 to 435 nm and 485 to 575 nm. The first-derivative curve for hematite exhibits a peak at 575 nm and that for goethite at 535–545 nm and 435 nm (Fig. 5b). When hematite and goethite occur together, which is typical in nature, their spectral curves overlap and reinforce each other (Balsam and Damuth, 2000). The net effect is that the hematite peak shifts toward shorter wavelengths, broadening the area under the peak and producing a shoulder at 525–535 nm (Balsam and Damuth 2000). Hence, Factor 2 is interpreted as the hematite + goethite factor. This interpretation is bolstered by the similarity of the shapes of the Factor 2 pattern curve and the hematite/goethite factor identified by Damuth and Balsam (2003). The down-core variations of Factor 2 pattern and S-ratio values also confirm the interpretation: The trends of Factor 2 pattern and S-ratio values (which indicate the relative proportions of magnetically "hard" and "soft" minerals) are very similar (Fig. 6 where S-ratio is plotted on a reverse scale for ease of comparison), indicating the anti-correlation between them. As Factor 2 indicates magnetically "hard" minerals and S-ratio values magnetically "soft" minerals, the negative correlation between them is expected ($r = -0.31$, $p = 0.10$, $n = 30$). This factor also exhibits a negative correlation with

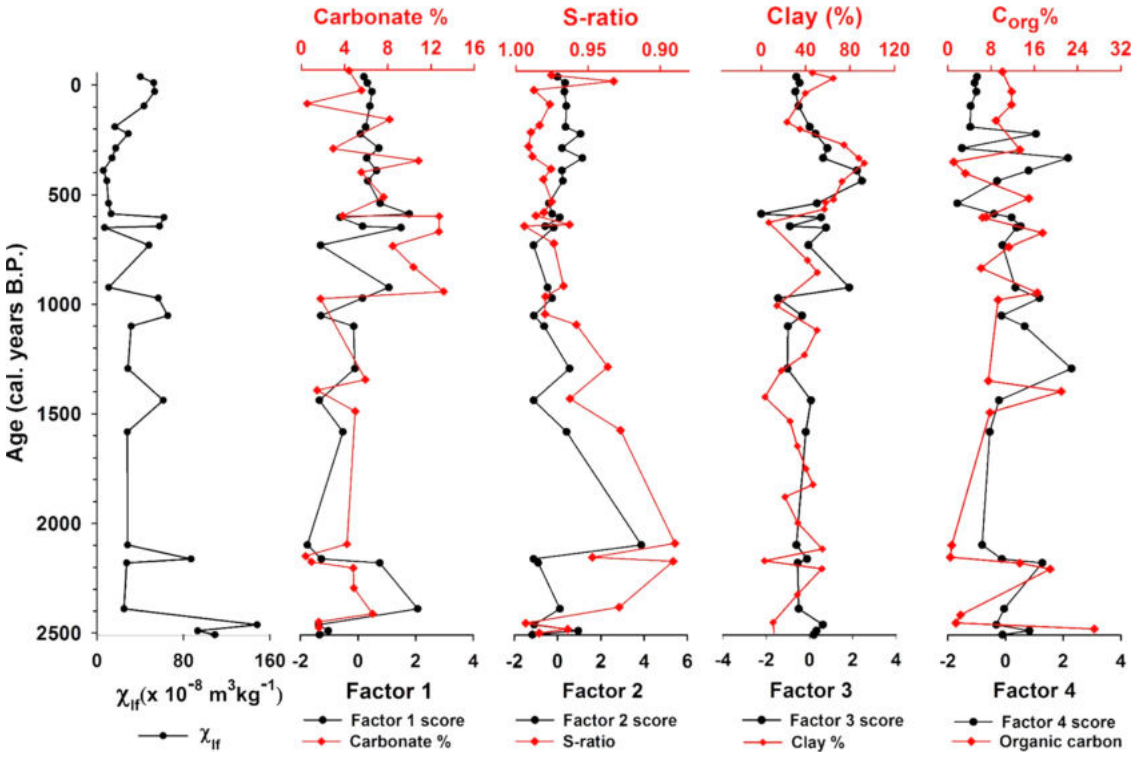

Figure 6. Down-core variations of χ_{lf} and Factor scores. Factors 1, 2, 3, and 4 are interpreted as carbonate, hematite/goethite, and clay and organic matter contents whose down-core variations are also shown (red lines). Note the close similarity of the trends of factor scores and the factor-interpreted component obtained by actual analysis. The scale for S-ratio is reversed for interpretational ease.

χ_{lf} (r = –0.35, p = 0.06, n = 30). Factor 2 scores range from –1.75 to 2.07. High positive values are documented for periods typified by low χ_{lf} and low S-ratio values (= periods of low rainfall). Low negative values are recorded for periods characterized by high χ_{lf} and high S-ratio values (= periods of high rainfall).

Factor 3

Factor 3 is a positive factor with major peaks at 275–305 nm (with factor loadings of 0.8 to 0.73) and 375–345 nm and a minor one at 455 nm. As the highest loadings are at the violet end of the spectrum, Factor 3 is identified as clay mineral factor, possibly a combination of montmorillonite and illite. The Factor 3 pattern curve (Fig. 5c) is similar to that reported by Balsam and Deaton (1991) and Damuth and Balsam (2003) for clay minerals. The peaks in the range 275–305 nm and 375–345 nm may indicate both montmorillonite and illite whereas the one at 455 nm matches closely with the illite peak (Damuth and Balsam, 2003). But an exact match is unlikely as clay minerals exhibit a wide range in composition (Damuth and Balsam, 2003). This is further substantiated by sedimentological data on the same samples (Bhattacharyya et al., 2015) and the similarity of down-core variations of clay percentage and the Factor 3 pattern curve (Fig. 6). Factor 3 scores range from –2.23 to 2.42. High positive values are documented for periods with low χ_{lf} values and high clay percentage (= periods of low rainfall) and low negative values during periods with high χ_{lf} values and low clay % (= periods of high rainfall). Usually, a high clay content is indicative of arid and low rainfall conditions (Chen et al., 2004; Peng et al., 2005; Conroy et al., 2008). The factor has a low negative correlation with χ_{lf} (r = –0.15) whereas clay has a more negative 'r' value with χ_{lf} (r = –0.71). A possible reason for this difference may be that lake sediments are a complex mixture of components and the spectra may not respond to in proportion to a component's weight (Balsam and Damuth, 2000). The dominant spectral signal in a factor may not necessarily be the component with the highest weight concentration due to differing spectral strengths (Balsam and Beeson, 2003).

Factor 4

Factor 4 is a positive factor too and has high loadings from 595 to 665 nm (peaking at 655 nm with a maximum factor loading of 0.78). The Factor 4 pattern curve (Fig. 5d) is similar to that reported by Damuth and Balsam (2003) for organic matter. Balsam and Deaton (1991) and Balsam and Wolhart (1993) identified first-derivative values that increase toward the red end of the spectrum (increased reflectance) and decrease at the violet end (increased absorption), which is typical of organic matter. The precise pattern produced by organic matter is a function of its type and concentration (Balsam and Damuth, 2000). Organic matter encompasses a wide variety of materials with differing spectral characteristics depending on their source and degree of maturation (Balsam and Beeson, 2003). As noted by Balsam and Deaton (1996) and Deaton et al. (1996), immature organic matter (which is not subjected to heat or pressure or intense bacterial action) has a golden brown colour. As organic matter ages and is subjected to increasing heat and pressure, it becomes darker and the absorption band gradually moves across the VIS towards the red end of the spectrum. Fully mature organic matter is black and absorbs through the entire VIS range. Factor 4 exhibits high first-derivative values at the red end of the spectrum, suggesting that this factor is the organic matter factor. This interpretation is corroborated by similar down-core variations of organic carbon, obtained from a CHN analyser, and Factor 4 loadings (Fig. 6). The two curves match well, particularly for the pre- ~1000 cal. years B.P. period. The organic matter content and Factor 4 loadings exhibit significant down-core variations; there are periods characterised by high and low organic matter content. Factor 4 scores range from –1.67 to 2.29. There is no correlation between both χ_{lf} and Factor 4 scores (r = –0.03) or organic carbon and χ_{lf} (r = 0.04). However, there are some periods when high χ_{lf} is associated with high Factor 4 scores and high organic carbon content.

The reason for the negative correlation between reflectance and susceptibility is the influence of Factor 1, i.e., the carbonate content. Carbonate is light coloured and hence increases the reflectance when present, the degree of increase in reflectance depending on carbonate concentration and the amount of dark minerals. As carbonate content (Factor 1) was high during periods characterised by low susceptibility values (= low rainfall) and vice versa, they have an inverse relation. But hematite content also exhibits a negative correlation with χ_{lf}. Therefore, reflectance should increase during periods typified by high χ_{lf} values (= high rainfall) because of the absence of dark minerals like hematite/goethite. Factor 2 exhibits a correlation coefficient of only –0.35 with χ_{lf} and –0.67 with Factor 1. This suggests that the reflectance signal of the PK samples is mainly controlled by Factor 1 rather than Factor 2. This is substantiated by the fact that from 1000 cal. years B.P. to 2500 cal. years B.P. Factor 1 scores (carbonate) are low and Factor 2 (haematite) scores are high. In other words, the reflectance and colour of Pookot Lake sediments are controlled mainly by the content of light coloured carbonates and not of dark coloured hematite/goethite.

Factor analysis reveals that colour variations in Pookot Lake sediment are indeed determined by the relative concentrations of a variety of sediment components, including organic matter, carbonate, clay and iron oxides. The results of DRS corroborate the data (carbonate content, particle size, organic carbon and rock magnetic properties) obtained from independent analyses, lending strength to the interpretations made in this study. Among the iron oxides, magnetite cannot be detected using DRS techniques. However, maghemite, which is dark brown, could be detected as Factor 5 with characteristic peaks at 595 and 665 nm (Damuth and Balsam, 2003). It explains only 1.3% of the cumulative variance and has an eigenvalue < 1.

Palaeoenvironmental history of the area

Around 2500 cal. years B.P. period

Around 2500 cal. years B.P., χ_{lf} and S-ratio display high values, which indicate strong pedogenesis and a high detrital influx of magnetite from the Pookot catchment. The presence of magnetically "soft" minerals is further substantiated by DRS data. Percentage redness and Hm565 values are low with low Factor 2 scores (indicative of hematite/goethite) for this period. The carbonate content is low, which is also confirmed by the low Factor 1 scores (indicative of carbonate). The clay percentage is low also. These data indicate relatively low rainfall around ~2500 cal. years B.P.

2500–1000 cal. years B.P. period

During this period, χ_{lf} and S-ratio exhibit low values. These characteristics point to a low influx of detrital magnetite to the lake and weak pedogenesis in the catchment. DRS data also exhibit an increased percentage redness and Hm565 values. Clay and carbonate contents are relatively high, which is substantiated by the high Factor 1 scores. However, this period is interspersed by short intervals with sharp peaks in χ_{lf} and S-ratio values but with decreased values of redness %, clay and carbonate contents. These data suggest that the period was characterized by low and steady rainfall, but interspersed with brief spells of high rainfall.

1000 cal. years B.P. to the Present period

The 1000–600 cal. years B.P. period is characterized by increasing trends of χ_{lf} and S-ratio values with a low percentage redness and Hm565 (–0.001) values. The clay content is high, although it displays a slightly decreasing trend. Carbonate content also exhibits a decreasing trend. The 1000–600 cal. years B.P. age bracket is the Medieval Warm Period (MWP) documented in many paleoclimatic records (Agnihotri et al., 2002; Brazdil et al., 2005). After the MWP, χ_{lf} values become remarkably low and S-ratio values relatively low, indicating a decreased influx of detrital magnetite and low pedogenesis in the catchment area. The clay content is high but the carbonate and organic carbon contents fluctuate. Overall, the rainfall was significantly lower during 600–350 cal. years B.P., which corresponds to the Little Ice Age (LIA). After 350 cal. years B.P., rainfall exhibits an increasing trend up to the Present. There is no agreement on the duration of LIA; its termination has been placed variously at 1700, 1850 or 1900 A.D. (Lamb, 1977). Although LIA is conventionally defined as the 16^{th} to mid-19^{th} century period when European climate was most strongly impacted, its timing and the nature of climatic fluctuations are highly variable from region to region and not synchronous globally (Mann, 2002). The Little Ice Age seems to be short-lived in the region as suggested by Fleitmann et al. (2004) and may be placed in the age bracket 1400–1600 A.D. (550–350 cal. years B.P.). But the period 1600–1750 A.D. (350–200 cal. years B.P.) experienced rainfall conditions weaker than the present, although it displays an increasing trend. Hence, the termination of LIA may not be exactly around 1600 A.D. (350 cal. years B.P.), but somewhere between 1600 and 1750 A.D. (350–200 cal. years B.P.).

Conclusions

In this study, we have highlighted the use of diffuse reflectance spectroscopic parameters to identify different components of lake sediments. The four dominant components of Pookot Lake sediments are carbonate, hematite/goethite, organic carbon and clay minerals. The components identified based on DRS techniques are independently validated by data obtained from other analyses. Based on down-core variations of the four components and χ_{lf} values (indicative of detrital magnetite), the paleoenvironmental history of the Pookot Lake catchment is reconstructed. Around 2500 cal. years B.P. the monsoon was strong compared to the Present. During 2500–1000 cal. years B.P., the monsoon was weak and steady, but interspersed with short spells of high rainfall. During 1000 cal. years B.P. to the Present, rainfall exhibits fluctuating trends. Rainfall was relatively high during the Medieval Warm Period (1000–600 cal. years B.P.) and low during the Little Ice Age (600–350 cal. years B.P.). From 350 cal. years B.P. to the Present, rainfall exhibits an increasing trend.

Acknowledgements

KS thanks the University Grants Commission, New Delhi, for financial assistance in the form of Junior and Senior Research Fellowships. AKW thanks the Council of Scientific and Industrial Research, Government of India, for a senior research fellowship. The authors thank the Sophisticated Analytical Instrumental Facility (SAIF), CUSAT, Cochin for providing access to elemental analyzer. The magnetic instruments used in this study were procured from grants made available by the erstwhile Department of Ocean Development (now Ministry of Earth Sciences), Government of India, through a research project (DOD/11-MRDF/1/48/P/94-ODII/ 12-10-96) to RS. We are grateful to two anonymous reviewers and the editor, EPISODES for their comments.

References

Agnihotri, R., Dutta, K., Bhushan, R., and Somayajulu, B.L.K., 2002, Evidence for solar forcing on the Indian monsoon during the last millennium: Earth and Planetary Science Letters, v.198, pp. 521–527.

Arimoto, R., Balsam, W., and Schloesslin, C., 2002, Visible spectroscopy of aerosol particles collected on filters: iron-oxide minerals: Atmospheric Environment, v.36, pp. 89–96.

Balsam, W.L., Ji, J., Renock, D., Deaton, B.C., and Williams, E., 2014, Determining hematite content from NUV/Vis/NIR spectra: Limits of detection: American Mineralogist, v.99 nos.11–12, pp. 2280–2291.

Balsam, W.L., and Beeson, J.P., 2003, Sea-floor sediment distribution in the Gulf of Mexico: Deep-Sea Research Part I, v.50, pp. 1421–1444.

Balsam, W.L., and Damuth, J.E., 2000, Further investigations of shipboard vs. shore-based spectral data: implications for interpreting Leg 164 sediment composition [A], in Paull, C.K., Matsumoto, R., Wallace, P.J., and Dillon, W.P., eds., Proceedings ODP scientific results, Texas: Ocean Drilling Program, Texas A and M University, v. 64, pp. 313–324.

Balsam, W.L., and Deaton, B.C., 1991, Sediment dispersal in the Atlantic Ocean: evaluation by visible light spectra: Reviews in Aquatic Sciences, v.4, pp. 411–447.

Balsam, W.L., and Deaton, B.C., 1996, Determining the composition of late Quaternary marine sediments from NUV, VIS, and NIR diffuse reflectance spectra: Marine Geology, v.134, pp. 31–55.

Balsam, W.L., and Wolhart, R.J., 1993, Sediment dispersal in the Argentine basin: evidence from visible light spectra: Deep Sea Research II, v.40, nos.4–5, pp. 1001–1031.

Balsam, W.L., Deaton, B.C., and Damuth, J.E., 1998, The effects of water content on diffuse reflectance spectrophotometry studies of deep-sea sediment cores: Marine Geology, v.149, pp. 177–189.

Balsam, W.L., Deaton, B.C., and Damuth, J.E., 1999, Evaluating optical lightness as a proxy for carbonate content in marine sediment cores: Implications for marine sedimentation: Marine Geology, v.161, pp. 141–153.

Balsam, W.L., Ellwood, B.B., Ji, J., Williams, E.R., Long, X., and Hassani, A.E., 2011, Magnetic susceptibility as a proxy for rainfall: worldwide data from tropical and temperate climate: Quaternary Science Reviews,

v.30, pp. 2732–2744.

Beuning, K.R.M., Talbot, M.R., Livingstone, D.A., and Schmukler, G., 2003, Sensitivity of carbon isotopic proxies to paleoclimatic forcing: A case study from Lake Bosumtwi, Ghana, over the last 32,000 years: Global Biogeochemical Cycles, v.17, no.4. DOI: 10.1029/2003GB002072.

Bhattacharyya, A., Sandeep, K., Sandhya, M., Shankar, R., Warrier, A.K., Weijian, Z., and Xuefeng, L., 2015, Vegetational and climatic variations during the past 3100 years in southern India: Evidence from pollen, magnetic susceptibility and particle size data: Environmental Earth Sciences, v.74, pp. 3559–3572.

Blaauw, M., 2010, Methods and code for 'classical' age-modelling of radiocarbon sequences: Quaternary Geochronology, v.5 no.5, pp. 512–518.

Bonnefille, R., Anupama, K., Barboni, D., Pascal, J.P., Prasad, S., and Sutra, J.P., 1999, Modern pollen spectra from tropical South India and Sri Lanka: Journal of Biogeography, v.26, pp. 1255–1280.

Brazdil, R., Pfister, C., Wanner, H., von Storch H., and Luterbacher, J., 2005, Historical climatology in Europe – the state of the art: Climate Change, v.70, pp. 363–430.

Chandran, P.P., 2003, District Handbooks of Kerala-Wayanad, in Rajasekharan, G., and Santhosh Kumar, K. eds., Department of Information and Public Relations, Govt. of Kerala.

Chen, J., Wan, G., Zhang, D.D., Zhang, F., and Huang, R., 2004, Environmental records of lacustrine sediments in different time scales: Sediment grain size as an example: Science in China (Series D - Earth Sciences), v.47, pp. 954–960.

Chengjun, Z., Zhaodong, F., Qili, Y, Xiaohui, G., and Feifei, S., 2010, Holocene environmental variations recorded by organic-related and carbonate-related proxies of the lacustrine sediments from Bosten Lake, northwestern China: The Holocene, v.20, pp. 363–373.

Colombo, C., Palumbo, G., Iorio, E.D., Russo, F., Terribile, F., Jiang, Z., and Liu, Q., 2015, Soil development in a Quaternary fluvio-lacustrine paleosol sequence in Southern Italy: Quaternary International. http://dx.doi.org/10.1016/j.quaint.2015.11.004.

Conroy, J.L., Overpeck, J.T., Cole, J.E., Shanahan, T.M., and Steinitz-Kannan, M., 2008, Holocene changes in eastern tropical Pacific climate inferred from a Galápagos lake sediment record: Quaternary Science Reviews, v.27, pp. 1166–1180.

Cornell, R.M., and Schwertmann, U., 1996, The iron oxides: VCH, New York, 573 p.

Cortina, A., and Herguera, J.C., 2014, Mid-to-Late Holocene organic carbon export variability at the southern boundary of the California Current: An approach based on diffuse spectral reflectance of marine sediment cores: Palaeogeography, Palaeoclimatology, Palaeoecology, v.408, pp. 1–10

Damuth, J.E., and Balsam, W.L., 2003, Data report: Spectral data from sites 1165 and 1167 including the HiRISC section from Hole 1165B, in Cooper, A.K., O'Brien, P.E., and Richter, C., eds., Proceedings of Ocean Drilling Program, Scientific Results, v.188, pp. 1–49.

Deaton, B.C., and Balsam, W.L., 1991, Visible spectroscopy – a rapid method for determining hematite and goethite concentration in geological materials: Journal of Sedimentary Petrology, v.61, pp. 628–632.

Deaton, B.C., Nestell, M., and Balsam, W.L., 1996, Spectral reflectance of conodonts: a step toward quantitative color alteration and thermal maturity indexes: American Association of Petroleum Geologists Bulletin, v.80, pp. 999–1007.

Dong, Y., Zhang, W., Dong, C., Ge, C., and Yu, L., 2014, Magnetic and diffuse reflectance spectroscopic characterization of iron oxides in the tidal flat sequence from the coastal plain of Jiangsu Province, China: Geophysical Journal International, v.196, pp. 175–188.

Duan, Z., Liu, Q., Yang, X., Gao, X., and Su, Y., 2014, Magnetism of the Huguangyan Maar Lake sediments, Southeast China and its paleoenvironmental implications: Palaeogeography, Palaeoclimatology, Palaeoecology, v.395, pp. 158–167.

Fang, X., Zan, J., Appel, E., Lu, Y., Song, C., Dai, S., and Tuo, S., 2015, An Eocene–Miocene continuous rock magnetic record from the sediments in the Xining Basin, NW China: indication for Cenozoic persistent drying driven by global cooling and Tibetan Plateau uplift: Geophysical Journal International, v.201, pp. 78–89.

Fleitmann, D., Burns, S.J., Neff, U., Mudelsee, M., Mangini, A., and Matter, A., 2004, Palaeoclimatic interpretation of high-resolution oxygen isotope profiles derived from annually laminated speleothems from Southern Oman: Quaternary Science Reviews, v.23, pp. 935–945.

Frank, U., 2007, Rock magnetic studies on sediments from Erlongwan Maar Lake, Long Gang Volcanic Field, Jilin province, NE China: Geophysical Journal International, v.168, no.1, pp. 13–26.

Geological and Mineral Map of Kerala, 1995, Compiled by Mallikarjuna, C., Nair, M.M., Gopalakrishnan, L.S., Adiga, K.S., Nambiar, A.R., Balakrishnan, P. et al.: Geological Survey of India, Scale 1:500000, 1 sheet.

Heslop, D., 2009, On the statistical analysis of the rock magnetic S-ratio: Geophysical Journal International, v.178, pp. 159–161.

India Meteorological Department, 2008, Rainfall data for Vythiri Station. Government of India, New Delhi.

Ji, J., Balsam, W., and Chen, J., 2001, Mineralogic and climatic interpretations of the Luochuan Loess Section (China) based on diffuse reflectance spectrophotometry: Quaternary Research, v.56, pp. 23–30.

Ji, J., Shen, J., Balsam, W., Chen, J., Liu, L., and Liu, X., 2005, Asian monsoon oscillations in the northeastern Qinghai–Tibet Plateau since the late glacial as interpreted from visible reflectance of Qinghai Lake sediments: Earth and Planetary Science Letters, v.233, pp. 61– 70.

Jiang, Z., Liu, Q., Colombo, C., Barrón, V., Torrent, J., and Hu, P., 2014, Quantification of Al-goethite from diffuse reflectance spectroscopy and magnetic methods: Geophysical Journal International, v.196, no.1, pp. 131–144.

Kerala Forest Department, 1986, Working plan report for the Kozhikode Forest Division. Department of Forests, Thiruvananthapuram, Government of Kerala.

Kruiver, P.P., and Passier, H.F., 2001, Coercivity analysis of magnetic phases in sapropel S1 related to variations in redox conditions, including an investigation of the S-ratio: Geochemistry, Geophysics, Geosystems, v.2. doi:10.1029/2001GC000181

Lee, C.Y., Liew, P.M., and Lee, T.Q., 2010, Pollen records from southern Taiwan: implications for East Asian summer monsoon variation during the Holocene: The Holocene, v.20, pp. 81–89.

Leng, M.J., and Marshall, J.D., 2004, Palaeoclimate interpretation of stable isotope data from lake sediment archives: Quaternary Science Reviews, v.23, pp. 811–831.

Liying, S., Weiling, S., and Jinren, N., 2009, Partitioning of water soluble organic carbon in three sediment size fractions: Effect of the humic substances: Journal of Environmental Sciences, v.21, pp. 113–119.

Lyons, R., Tooth, S., and Duller, G.A.T., 2014, Late Quaternary climatic changes revealed by luminescence dating, mineral magnetism and diffuse reflectance spectroscopy of river terrace palaeosols: a new form of geoproxy data for the southern African interior: Quaternary Science Reviews, v.95, pp. 43–59.

Mann, M.E., 2002, Little Ice Age. Vol. 1, The Earth system: physical and chemical dimensions of global environmental change, in MacCracken, M.C., and Perry, J.S., eds., Encyclopedia of Global Environmental Change. pp. 504–509.

Meyers, P.A., and Lallier-Verges, E., 1999, Lacustrine sedimentary organic matter records of Late Quaternary paleoclimates: Journal of Paleolimnology, v.21, pp. 345–372.

Mohanty, B., Gupta, A., and Das, B.S., 2016, Estimation of weathering indices using spectral reflectance over visible to mid-infrared region: Geoderma, v.266, pp. 111–119.

Oliveira, S.M.B., Gouveia, S., Pessenda, L.C.R., and Favaro, D.I.T., 2009, Lacustrine sediments provide geochemical evidence of environmental change during the last millennium in southeastern Brazil: Chemie der Erde-Geochemistry, v.69, no.4, pp. 395–405.

Peng, Y., Xiao, J., Nakamura, T., Liu, B., and Inouchi, Y., 2005, Holocene East Asian monsoonal precipitation pattern revealed by grain-size distribution of core sediments of Daihai Lake in Inner Mongolia of north-central China: Earth and Planetary Science Letters, v.233, pp. 467–479.

R Development Core Team, 2010, R: A language and environment for statistical computing. R Foundation for Statistical Computing, Vienna Austria. ISBN 3-900051-07-0. http://www.R-project.org

Reimer, P.J., Baillie, M.G.L., Bard, E., Bayliss, A., Beck, J.W., Blackwell, P.G., Bronk Ramsey, C., Buck, C.E., Burr, G.S., Edwards, R.L., Friedrich, M., Grootes, P.M., Guilderson, T.P., Hajdas, I., Heaton, T.J., Hogg, A.G., Hughen, K.A., Kaiser, K.F., Kromer, B., McCormac, F.G., Manning, S.W., Reimer, R.W., Richards, D.A., Southon, J.R., Talamo, S., Turney, C.S.M., van der Plicht, J., and Weyhenmeyer, C.E., 2009, IntCal09 and Marine09 radiocarbon age calibration curves 0-50000 years cal. BP: Radiocarbon, v.51, pp. 1111–1150.

Sandeep, K., Shankar, R., Warrier, A.K., Weijian, Z., and Xuefeng, L., 2015, The environmental magnetic record of palaeoenvironmental variations during the past 3100 years: A possible solar influence?: Journal of Applied Geophysics, v.118, pp. 24–36.

Schumacher, B.A., 2002, Methods for the dtermination of total organic carbon (TOC) in soils and sediments: Ecological Risk Assessment Support Center, Office of Research and Development, US. Environmental Protection Agency, 23 p.

Shankar, R., Prabhu, C.N., Warrier, A.K., Vijaya Kumar, G.T., and Sekar, B., 2006, A multi-decadal rock magnetic record of monsoonal variations during the past 3700 years from a tropical Indian tank: Journal of the Geological Society of India, v.68, pp. 447–459.

Soman, K., 1997, Geology of Kerala: Geological Society of India, Bangalore, 280 p.

Srivastava, P., Sangode, S.J., and Torrent, J., 2015, Mineral magnetic and diffuse reflectance spectroscopy characteristics of the Deccan volcanic bole beds: Implications to genesis and transformations of iron oxides: Geoderma, v.239–240, pp. 317–330.

Stober, J.C., and Thompson, R., 1979, An investigation into the source of magnetic minerals in some Finnish lake sediments: Earth and Planetary Science Letters, v.45, pp. 464–474.

Torrent, J. and Barrón, V., 2002, Diffuse reflectance spectroscopy of iron oxides. Encyclopedia of Surface and Colloid Science, pp. 1438-1446.

Trivedi, A., and Chauhan, M.S., 2008, Pollen proxy records of Holocene vegetation and climate change from Mansar Lake, Jammu region, India: Current Science, v.95, no.9, pp. 1347–1354.

Walden, J., 1999, Sample collection and preparation, in Walden, J., Smith, J.P., and Oldfield, F., eds., Environmental Magnetism – A practical guide. Technical Guide No. 6, Quaternary Research Association, London, pp. 26–34.

Warrier, A.K., and Shankar, R., 2009, Geochemical evidence for the use of magnetic susceptibility as a paleorainfall proxy in the tropics: Chemical Geology, v.265, pp. 553–562.

Warrier, A.K., Shankar, R., and Sandeep, K., 2014a, Sedimentological and carbonate data evidence for lake level variations during the past 3700 years from a Southern Indian lake: Palaeogeography, Palaeoclimatology, Palaeoecology, v.397, pp. 52–60.

Warrier, A.K., Mahesh, B.S., Mohan, R., Shankar, R., Asthana, R., and Ravindra, R., 2014b, Glacial-interglacial climatic variations at the Schirmacher Oasis, East Antarctica: The first report from environmental magnetism: Palaeogeography, Palaeoclimatology, Palaeoecology, v.412, pp. 249–260.

Wei, J.H., Finkelstein, D.B., Brigham-Grette, J., Castaneda, I.S., and Nowaczyk, N., 2014, Sediment colour reflectance spectroscopy as a proxy for wet/dry cycles at Lake El'gygytgyn, Far East Russia, during Marine Isotope Stages 8 to 12: Sedimentology, v.61, no.6, pp. 1793–1811.

Zhang, E., Sun, W, Ji, M., Zhao, C., Xue, B., and Shen J., 2015, Late Quaternary carbon cycling responses to environmental change revealed by multi-proxy analyses of a sediment core from an upland lake in southwest China: Quaternary Research, v.84, pp. 415–422.